Characterization of AlScN-Based Multilayer Systems for Piezoelectric Micromachined Ultrasound Transducer (pMUT) Fabrication

Kristina Bespalova, *Member, IEEE*, Elmeri Österlund, Glenn Ross, *Member, IEEE*, Mervi Paulasto-Kröckel, *Member, IEEE,* Abhilash Thanniyil Sebastian, Cyril Baby Karuthedath, Stefan Mertin, *Member, IEEE*, and Tuomas Pensala, *Member, IEEE*

***Abstract*— Scandium-alloyed aluminum nitride (AlScN) is a potential material for micro-electromechanical systems because of its unique advantages, such as strong piezoelectric effect and high thermal stability. However, issues related to its stability and interaction with other materials in multilayer systems require investigation. The formation of new phases at the interface between piezomaterial and electrode material can lead to the device failure. In this study, multilayer structures Si substrate/AlN/Ti-Mo/$Al_{0.8}$ $Sc_{0.2}N$/top electrode (TE) were studied after annealing at a wide range of temperatures and durations. Four different TE materials (i.e. Al, AlSi (1%), Mo/Al, and Mo) were examined to determine the most reliable electrode material for the structure. The phase stability, interfacial quality, and piezoelectric response of the multilayer systems after thermal annealing were investigated. The structure with Mo TE layer was stable after annealing at 800 °C for 300 h and at 1000 °C for 100 h. None of the structures formed any new phases at the interface between the electrode layer and AlScN. The transverse piezoelectric coefficient ($e_{31,f}$) was determined for $Al_{0.8}Sc_{0.2}N$ before and after annealing. The absolute value of the $e_{31,f}$ was −1.39 C/m^2 for as-deposited structure and −1.67 C/m^2 for the same structure annealed for 300 h at 800 °C. [2020-0361]**

***Index Terms*— AlScN, materials reliability, piezoelectricity, sputtered thin films.**

I. Introduction

PIEZOELECTRIC scandium-alloyed aluminum nitride (AlScN) thin films are considered an attractive material for use in microelectronics for the fabrication of piezo-driven energy harvesters [1], sensors [2], and surface and bulk acoustic wave devices [3]. Relatively high piezoelectric coefficients and thermal stability give AlScN advantage compared to perovskite-type piezoelectrics and piezoelectric polymers, which usually lose piezoelectric properties at high temperatures. Thermal stability of AlScN was described by Akiyama *et al.* in work [4], where was shown that AlScN did not lose piezoelectric properties after annealing at 580 °C for 56 h. In the same work [4] a significant increase in the piezoelectric response of scandium-alloyed AlN films was shown for the first time. It was shown, that piezoelectric coefficient $d_{33,f}$ gradually increases with increasing Sc concentration in the AlN film [4]. Subsequently, many studies have aimed to improve the piezoelectric properties [4]–[9] and optimize the material deposition process or device design [10]–[12].

Despite the attractiveness of AlScN, only c-axis oriented wurtzite AlScN can improve the performance of piezoelectric MEMS and replace industry standard AlN piezoelectric thin films. However, previous studies have shown instability of the wurtzite form for AlScN, especially for films with high Sc content [4], [13]–[15]. Exceeding the maximum concentration of Sc in AlScN leads to the formation of two-phase mixture regions and loss of the piezoelectric properties. In two-phase mixture region, two phases coexist simultaneously: wurtzite and cubic phase, where wurtzite has piezoelectric properties, and cubic does not. Transition from the wurtzite to two-phase mixture regions depends not only on the Sc concentration in the AlScN film but also the deposition conditions, residual stress, and environmental conditions [15]. Thus, Österlund *et al.* in work [16] showed formation of the rock-salt phase in $Al_{0.7}Sc_{0.3}N$ on the interface with Si induced by annealing in the vacuum.

Considering instability of AlScN, for device fabrication, it is important to evaluate how AlScN behaves when interacting with different types of materials, especially metallization materials. The piezoelectric layer cannot be used separately from other materials in piezoelectric components and is a part of an ordered multi-material structure with several interfaces. These interfaces provide potential for defect formation since different materials behave differently under changing external conditions. The coefficient of thermal expansion (CTE), residual film stresses, and interlayer diffusion differences can lead to the formation of new, undesirable phases on the

Manuscript received October 29, 2020; revised December 29, 2020; accepted January 26, 2021. Date of publication February 15, 2021; date of current version March 16, 2021. This work is part of the POSITION-II project funded by the ECSEL Joint Undertaking under grant number Ecsel-783132-Position-II-2017-IA (www.position-2.eu). The work of Kristina Bespalova was supported in part by funding from Aalto ELEC Doctoral School. Subject Editor L. Lin. *(Corresponding author: Kristina Bespalova.)*

Kristina Bespalova, Glenn Ross, and Mervi Paulasto-Kröckel are with the Department of Electrical Engineering and Automation, Aalto University, 02150 Espoo, Finland (e-mail: kristina.bespalova@aalto.fi).

Elmeri Österlund is with the Department of Electrical Engineering and Automation, Aalto University, 02150 Espoo, Finland, and also with Kyocera Tikitin Ltd., 02150 Espoo, Finland.

Abhilash Thanniyil Sebastian, Cyril Baby Karuthedath, Stefan Mertin, and Tuomas Pensala are with the VTT Technical Research Centre of Finland, 02150 Espoo, Finland.

Color versions of one or more figures in this article are available at https://doi.org/10.1109/JMEMS.2021.3056928.

Digital Object Identifier 10.1109/JMEMS.2021.3056928

This work is licensed under a Creative Commons Attribution-NonCommercial-NoDerivatives 4.0 License.
For more information, see https://creativecommons.org/licenses/by-nc-nd/4.0/

interfaces. These differences can also lead to compositional changes and, as a result, can negatively affect the operation of a device. Phase diagrams could provide information on the system's phase stability and the formation of phases at interfaces, as described in [17] by Laurila *et al.* However, a comprehensive thermodynamic description of the Al-Sc-N or higher order systems do not exist, such as ternary Al-Sc-N or quaternary X-Al-Sc-N (X-additional element) phase diagrams. As there is not detailed thermodynamic understanding of the x-Al-Sc-N, thermal stability studies like this are required to select the correct metallization material for microelectronic components containing AlScN piezoelectric layer. The choice of proper metallization would increase the devices' reliability and extend the lifetime of the product. Therefore, thermal stability studies of multilayer structures are essential for the design of devices in which AlScN could be used effectively. Temperature tests are important not only for devices used at high temperatures but also for accelerating potential system failures that occur over time in devices working under normal conditions. Although Schroeder *et al.* [18] published data for the limited thermal stability of a TiN/AlScN system due to interlayer diffusion, there is still a lack of studies on the interaction of AlScN with other types of materials and, especially, metallization materials. This work reports research on the stability of AlScN in combination with several metallization materials in a multilayer system under different annealing conditions.

In the structures under study, $Al_{1-x}Sc_xN$ (x = 0.2) was sandwiched between top electrode (TE) and bottom electrode (BE) layers. The thicknesses and sequence of the layers replicated a design used for the fabrication of piezoelectric micromachined ultrasonic transducers (pMUTs) in [19]. Al, AlSi (1%), Mo/Al, and Mo were utilized as the top electrode (TE) layers in the structures to examine the AlScN interaction with these metallization materials. The purpose of this study was to examine the phase stability, interfacial quality, and piezoelectric response of the multilayer systems after thermal annealing.

II. Materials and Methods

A. Sample Preparation

The thin-film layer stack was sputter deposited in a Von Ardenne CS 730 S sputtering system. The stack has following structure: Si substrate/AlN (1.2 μm)/Ti-Mo BE (20/150 nm)/$Al_{0.8}Sc_{0.2}N$ (1 μm)/TE, where TE = Al (500 nm), AlSi (1%) (500 nm), Mo/Al (300/100 nm), and Mo (300 nm), AlScN films. Molybdenum and AlScN were deposited at 450 °C and 300 °C respectively, all other TE were sputtered at room temperature. The annealing was carried out in vacuum with a base pressure of $<10^{-5}$ mbar in a vacuum furnace Webb Red Devil. A schematic of the layer structure and an example of a pMUT design that can be fabricated using this structure are presented in Fig. 1.

In addition to temperature, annealing duration is a driving factor for microstructural evolution [17]; therefore, the samples were divided into three sets. The first set of samples was annealed for 30 min at 100, 200, 300, 400, and 450 °C.

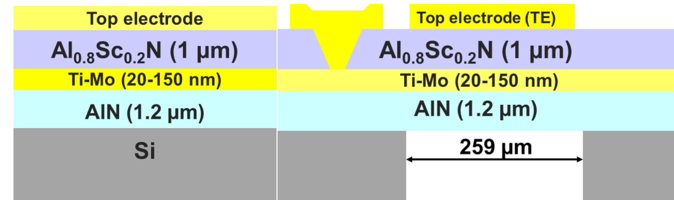

Fig. 1. Schematic illustration of the structures under study and pMUT structure which can be formed as an example. Top electrode X = Al (500 nm), AlSi (1%) (500 nm), Mo/Al (300/100nm), and Mo (300 nm).

TABLE I
Annealing Condition for Different Sets of the Samples

Set of the samples	Tested TE materials	Annealing temperature T, ℃	Annealing time t, h
I	Al, AlSi, Mo, Mo/Al	100 – 450	0.5
II	Al, AlSi, Mo, Mo/Al	450	50
III	Mo	450, 800, 1000	100, 100 – 300*

* only for the sample annealed at 800 ℃

This short-time annealing was done in order to examine the impact of different temperatures on the structures. The second set was annealed for 50 h at 450 °C. This long annealing duration at a high temperature was chosen to examine the effect of ageing on the structures. Since Mo is a much more thermostable material compared to the other metallization materials included in the study, the samples with Mo TE were exposed to harsher thermal stresses. Moreover, previous studies [8], [16] performed on films grown at similar deposition conditions have shown that the quality of AlScN films can be improved by annealing at high temperatures (i.e. 800 °C and 1000 °C). For this, a third set with Mo TEs was annealed at 450, 800, and 1000 °C for 100 h. Annealing condition for each set of the samples can be found in the Table I.

B. Characterization Methods

Morphology of the top layers was analyzed by a scanning electron microscopy (SEM) on a field-emission SEM JEOL JSM-6335F. Surface roughness of the samples was measured by an atomic force microscope (AFM) Bruker Dimension Icon using TESPA V2 probes.

The formation of new phases was determined by X-ray diffraction (XRD) analysis using a Rigaku SmartLab X-ray diffractometer with a 9 kW rotating Cu anode source. X-ray diffraction χ-2θ maps were constructed for both as-deposited and annealed samples. Diffractogram indexing was done using Inorganic Crystal Structure Database. To evaluate the AlScN film crystal quality, X-ray rocking curves (XRCs) were measured for both, as-deposited and annealed samples. Full width on half maximum (FWHM) values were determined for the obtained XRCs.

Electron-transparent lamellas were prepared using Focused Ion Beam SEM in a dual-beam JEOL JIB-4700F. Scanning transmission electron microscopy (STEM), selected area

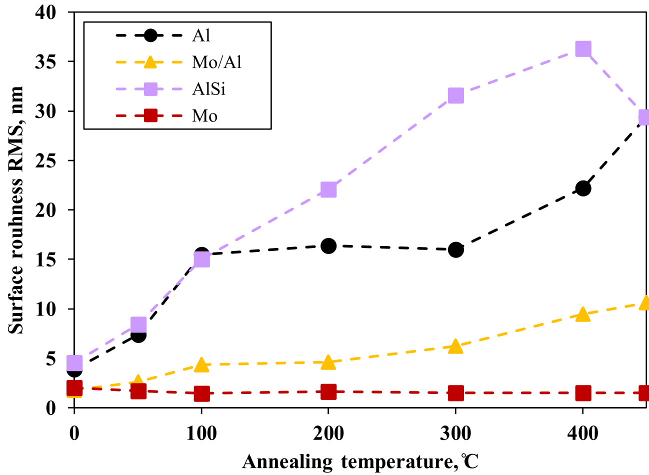

Fig. 2. RMS surface roughness R_q as a function of annealing temperature. All samples were annealed for 30 min.

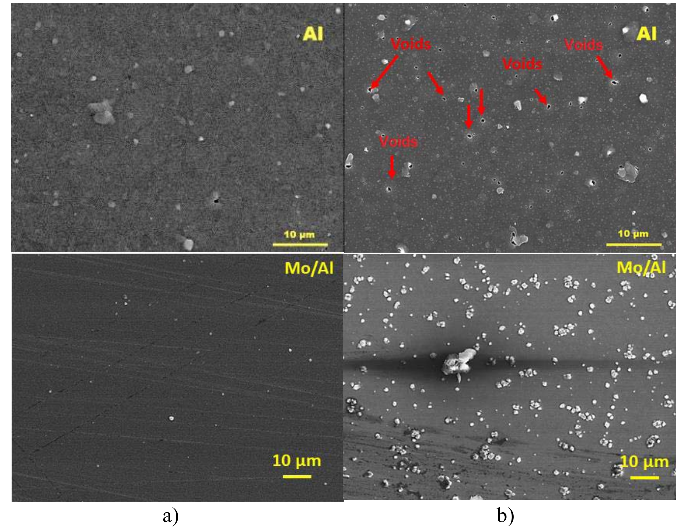

a) b)

Fig. 3. SEM images of samples with Al and Mo/Al top layers annealed at 450 °C for a) 30 min and b) 50 h.

electron diffraction (SAED), and energy-dispersive X-ray spectroscopy (EDX) mapping were used to acquire more accurate information on the metal/piezoelectric interface.

The transversal piezoelectric coefficient ($e_{31,f}$) of the AlScN films was determined measuring the cantilever displacement versus applied voltage acquired by a ferroelectric test system Precision LC II by applying ±30 V to piezo-cantilever electrodes.

C. Piezo-Cantilever Fabrication

A piezo-cantilever assembly consisting of plate capacitor structure was fabricated to measure the piezoelectric response of the structures. Molybdenum top layer etching was carried out in a phosphoric acid-based etching mixture 80:16:4 (65) (H_3PO_4:HNO_3:DI) at 50 °C for ~42 s. To access the Mo BE contact, AlScN etching was carried out in a 25 wt% potassium hydroxide (KOH) aqueous solution at 40 °C for 7 min. The AlScN etch rate strongly depends on the KOH solution temperature (i.e. it slows down with decreasing temperature). Therefore, 25 min was required to etch 1 μm of AlScN at room temperature. Phosphoric acid (H_3PO_4) can also be used for AlScN etching; AlScN etching in 85% H_3PO_4at 80 °C for structures with Pt electrodes has been reported [20]; however, $H_3PO_4$was not used in this study. After etching, the patterned plate-capacitor structures were diced into 4.5 mm × 72 mm cantilevers. For the TE different widths were used, 0.1 mm and 1 mm.

III. Results and Discussion

A. Surface Characterization

Aluminum, AlSi, and Mo thin film metallization were selected for the comparation in this study because they are the most used metallization materials. Sometimes Al is deposited on the contact pads forming Mo/Al structure for proper electrical connections, as Mo TEs have low electrical conductivity. To evaluate the effect of the thermal exposure, SEM micrographs of the top layer metallization were carried out after annealing for 30 min at 100, 200, 300, 400, and 450 °C. Hillocks tended to form on the surfaces of the top Al and AlSi layers during the annealing (see Fig. 10 in appendix A). The formation of hillocks in thin metal films is a well-known reliability problem in the microfabrication process [21]. The phenomenon of hillock formation is driven by the release of thermal-induced compressive stress, involving plastic deformation [21]–[23] and atomic diffusion [21] in metallic films. Compressive stress occurs in films because of mismatched coefficients of thermal expansion. The CTE for $Al_{1-x}Sc_xN$ ($x = 0.23$) is $4.95 \pm 0.26 \times 10^{-6}$ C^{-1} [24] and the CTE for Al thin films ranges from 18.23×10^{-6} C^{-1} to 29.97×10^{-6} C^{-1} [25]. The CTE for Mo is 5.56×10^{-6} C^{-1} [26]. Because of hillock nucleation, the extrusion of materials is often accompanied by the formation of voids or grooves in the film, and the formation of hillocks can cause electrical shorts in systems [27]. Several methods have been proposed to reduce hillock formation, including alloying. Aluminum alloying by Si, Ti, or Cu suppresses the growth of hillocks due to film hardening [28], [29]. Using thinner metal films can help decrease hillock grain size, hillock density over a substrate, and hillock volume per unit area because thinner films have higher yield strengths [22].

A gradual increase in the number and size of hillocks with elevated annealing temperature was observed for the samples with Al and AlSi metallization. Surface roughness was assessed by AFM measurement of a 30 μm × 30 μm scanning area for all the structures (see Fig. 2). The data in Fig.2 were in good agreement with the SEM micrographs and showed a rapid increase in RMS surface roughness with increasing annealing temperatures for samples with Al and AlSi top layers. Both the Al and AlSi layers were 500 nm thick, and the formation of hillocks in Al and AlSi grown on AlScN surface exhibited the similar behavior as Al grown on Si [17]. The size and number of the hillocks were almost linearly dependent on the annealing temperature. Hillocks started growing in all the films from 100 °C annealing temperature, except for Mo.

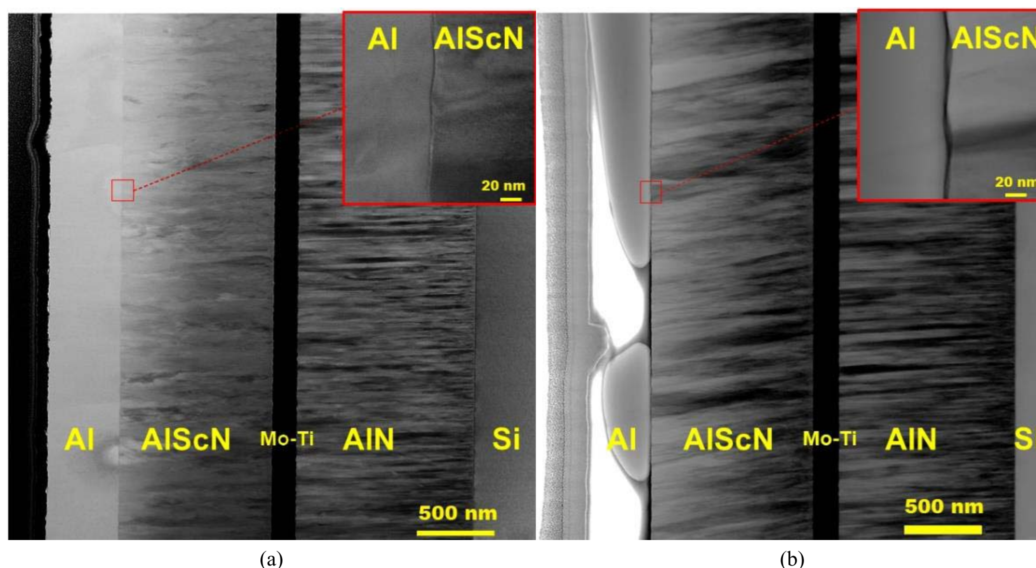

(a) (b)

Fig. 4. Cross-section STEM-BF micrographs of the Al/AlScN/Mo-Ti/AlN on Si structure. a) As-deposited and b) annealed at 450 °C for 50 h. Pt was used as a protective layer for lamella preparation (this can be seen on top of the Al layers).

Moreover, voids formation in Al film occurred after annealing at 200 °C. According to the AFM measurements, a void depth of approximately 15 nm was observed in the samples annealed at 200 °C and ranged from 60 to 211 nm for films annealed at 450 °C. Doping with Si (1 wt%) did not prevent the formation of hillocks in the AlSi film. However, void formation was not observed for samples with AlSi annealed up to 450 °C. Annealing time for all samples was 30 min.

For the Mo/Al top electrode, a decrease of thickness of the Al film and the use of Mo underlayer led to a reduction in the growth of hillocks, but it did not entirely prevent this process. The average height of the hillocks for the Mo/Al top layers annealed at 450 °C for 30 min was 200 nm for the Al and AlSi annealed in the same conditions. No hillocks were detected on the Mo surface, and its RMS surface roughness did not exceed 2 nm over the measured temperature range from 100 °C to 450 °C, which can be explained by the high thermal stability of this material.

The RMS surface roughness measurements of the top layers after a relatively long annealing time of 50 h at 450 °C were 1.5, 37.6, 103, and 197 nm for Mo, Al, AlSi, and Mo/Al, respectively. This indicated that the formation of the hillocks continued over time to a large extent for the Mo/Al and AlSi films, while the Al film did not significantly change over time. Figure 3 shows the changes in the Al and Mo/Al films after 50 h of annealing. The number of voids increased in the Al film after 50 h of annealing, while the Mo/Al films formed a much larger number of hillocks but remained intact.

B. Interface Characterization

To assess whether a new phase had formed in the systems after annealing and to evaluate the crystal quality over the sample area, χ-2θ XRD maps were used. A new reflection would mark the appearance of a new phase on the annealed sample maps compared to the reference sample. For all structures no new phases were found before and after annealing at 450 °C for 50 h, the extreme case of annealing. Appendix A contains the corresponding measured χ-2θ XRD maps. As expected, the diffraction space maps of the samples annealed for 30 min at 100–400 °C also did not indicate the presence of any foreign phases.

Although the AlScN films were c-axis oriented. The χ-2θ XRD maps of the non-annealed samples showed the presence of tilted AlScN grains relative to AlN. In some cases, the grain inclination exceeded 3 °. Most likely explanation for this non-uniform grain tilt was the deposition conditions. The structure with the Al top layer annealed at 450 °C for 50 h was chosen for the STEM analysis, which did not show any changes in the AlScN microstructure of the sample. In Fig. 4, the tilt of AlScN grains, which was absent in the images of the as-deposited sample, can be explained by the choice of the TEM lamella position on the sample's surface. The SAED pattern shown in Fig. 5 was recorded on the AlScN near the Al/AlScN interface. The lattice constants of the as-deposited $Al_{0.8}Sc_{0.2}N$ were a = 3.221 Å and c = 5.006 Å, calculated with the help of the SAED patterns using AlScN (0002) and AlScN (101'0) diffraction spots. The microstructure of the sample was unaffected by annealing at 450 °C for 50 h. TEM EDX mapping was used to investigate the possibility of interlayer diffusion between the Al and AlScN layers; however, no interlayer diffusion was found (Fig. 6). The presence of oxygen in the films was the result of natural oxidation at room temperature.

C. Piezoelectric Response Assessment

To assess the piezoelectric properties of the films, a set of piezo-cantilevers was produced of the structures with Mo top electrode as described in the materials and methods Section II.B. The transverse piezoelectric coefficient $e_{31,f}$ was measured as a function of piezo-cantilever displacement under

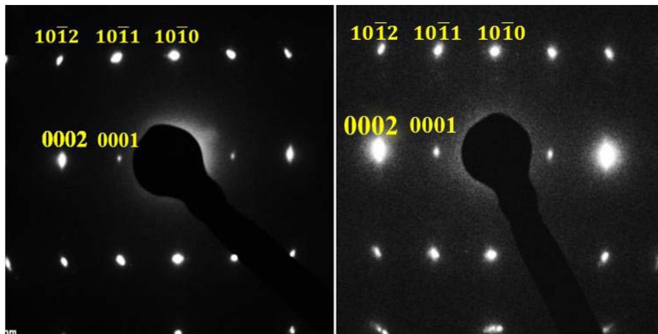

Fig. 5. SAED patterns of the Si/AlN/Ti-Mo/$Al_{0.8}Sc_{0.2}N$/Al structure. As-deposited (left) and annealed at 450 °C for 50 h (right). The images are contrast and brightness enhanced.

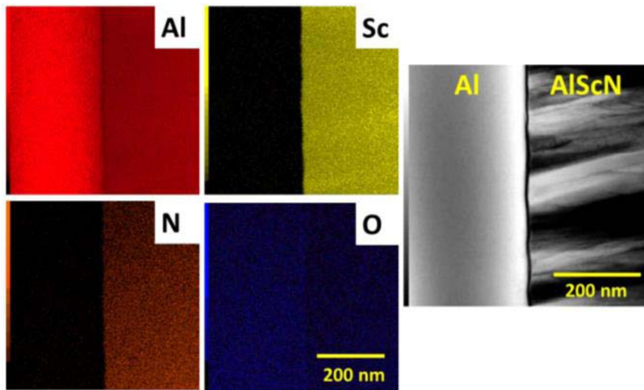

Fig. 6. EDX maps of the Al/AlScN interface after annealing at 450 °C for 50 h. Image contrast and brightness enhanced.

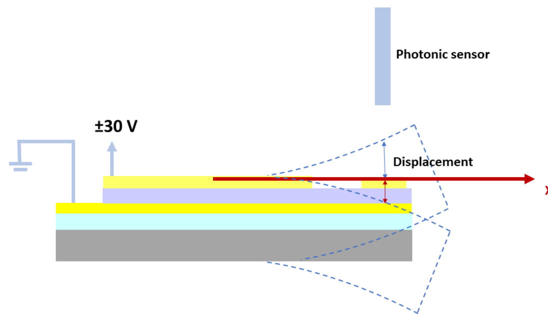

Fig. 7. Schematic cross-section illustrating the piezo-cantilever displacement measurement. The AlScN piezo layer is sandwiched between electrodes.

an applied voltage (Fig. 7). The transverse piezoelectric coefficient is an important parameter for structures with a membrane or beam structure. The following method for calculating the $e_{31,f}$ was used to minimize any error introduced into the measurements by ambient noise. For each piezo-cantilever, 100 consecutive displacement measurements were made, and an outputted displacement vs. voltage curve approximated the 100 measurements. This was carried out ten times in a row for each cantilever. Each of the ten curves obtained was fitted into Stoney equation as described in [30] to determine the value of $e_{31,f}$. Thus, the final values of $e_{31,f}$ shown in Fig. 8 are averaged values. The values of $e_{31,f}$ ranged from -1.39 C/m^2 to -1.65 C/m^2.

TABLE II
LOCATION OF THE $Al_{0.8}Sc_{0.2}N$ (0002) REFLECTION AND THE FWHM OF THE (0002) XRC OF THE FILMS BEFORE AND AFTER ANNEALING

Annealing conditions	2θ (°) AlScN	FWHM ω (°)
As-deposited	35.86	2.03
100 h, 800 ℃	35.70	2.72
200 h, 800 ℃	35.86	2.34
300 h, 800 ℃	35.86	2.32
100 h, 450 ℃	35.89	2.17
100 h, 1000 ℃	35.91	1.90

The AlScN grain tilt was unevenly distributed over the wafer. The change in the grain tilt over the wafer can be explained by the deposition condition and by the position of the deposition source with respect to the substrate in the sputtering system [31]. Thus, inclination of the grains in different parts of the wafer resulted in variations in the piezoelectric coefficient $e_{31,f}$ for the piezo-cantilevers fabricated on different parts of the wafer. Figure 8 shows the change in the grain tilt value accompanied by the change in the values of 2θ and χ for the AlScN (0002) reflection. The determined piezoelectric coefficients depended on the piezo-cantilever's position on the wafer, and the absolute value of the piezocoefficient decreased with increasing grain tilt. The measurements were done for the six cantilevers fabricated on a 6 inch wafer, where cantilever number 1 was formed close to the center of the wafer and cantilever number 6 almost at the edge of the wafer. Every cantilever was 4.5 mm × 72 mm in size. The values are in good agreement with the experimental and modeling data summarized by Mertin *et al.* [6].

Since the Mo TE material demonstrated best stability during the annealing, the stability of these structures was also tested at higher temperatures and longer annealing times.

According to the XRD results, there were no significant changes in the structure of the films after annealing. A notable broadening in the width of the XRC was observed for the sample annealed for 100 h at 800 °C. The grain inclination was preserved before and after annealing for all the samples. The FWHM data and the location of the $Al_{0.8}Sc_{0.2}N$ (0002) reflection are presented in Table II. The location of the AlN (0002) reflection was equal to $2\theta = 36.01°$ for as-deposited films and did not change after annealing.

Presumably, a small difference in the CTE values for Mo and AlScN created microstrain in the AlScN film during the first annealing for 100 h at 800 °C. However, continued annealing led to the relaxation of the microstrain, which was accompanied by a decrease in the FWHM value and the (0002) peak returning to the 35.86° position.

The effect of postdeposition thermal treatment for the enhancement of AlScN thin film piezoresponse has been studied earlier [8], [32]. An increase in the piezoelectric response was achieved by improved film quality, which was accompanied by a decrease in the FWHM value. The dependence of FWHM and $e_{31,f}$ on the annealing time at 800 °C for the structures is shown in Fig. 9. As the value of the FWHM for

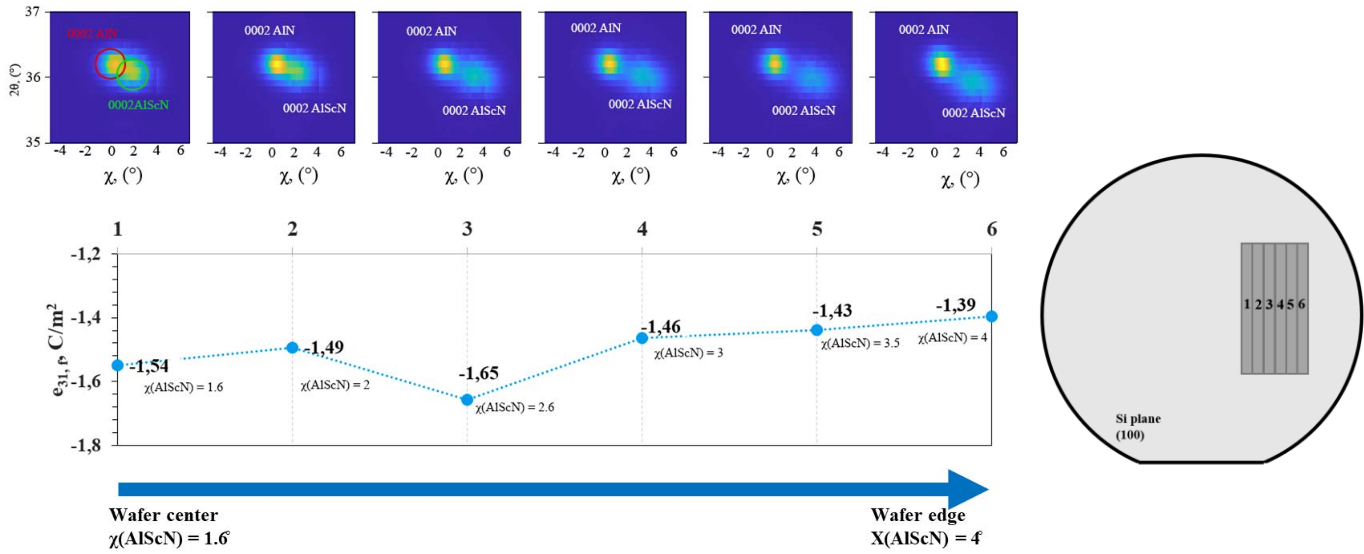

Fig. 8. Piezoelectric coefficient $e_{31,f}$ for the piezo-cantilevers formed at different parts of the wafer and χ-2θ XRD maps showing AlScN grain tilt values.

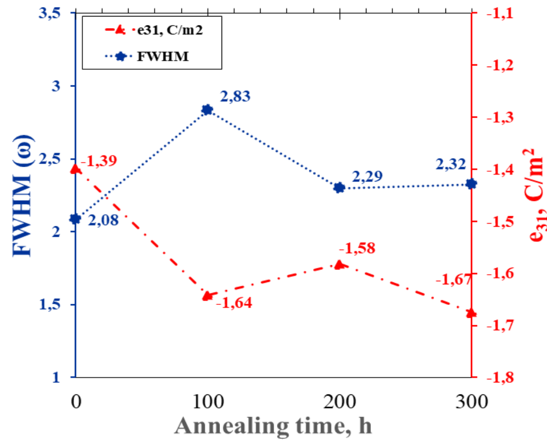

Fig. 9. FWHM and the piezoelectric coefficient $e_{31,f}$ as a function of film annealing time at 800 °C.

the (0002) XRC increased with annealing time, the absolute value of $e_{31,f}$ also increased.

Thus, the effect of piezoelectric response enhancement after heat treatment is driven by not only an improvement in crystal quality but also other internal phenomena. A possible explanation for the piezoresponse enhancement after annealing could be changes in the AlScN alloy configuration, namely the Al and Sc atom sites change under the influence of temperature. The impact of alloy configuration on the piezo-electric properties of the AlScN has been described in detail in works [33], [34]. Al and Sc atoms can occupy different lattice sites in the crystal, which affects stiffness of the material and strain sensitivity, which affects the piezoelectric constants.

Annealing the structure at 1000 °C slightly improved the crystal quality of the AlScN film and decreased the FWHM value from 2.03° to 1.90°. Nevertheless, also the surface of the Mo top layer after annealing for 100 h at 1000 °C was covered by grains (see Fig. 19 in appendix A). The XRD χ-2θ map of this structure did not show the presence of a new phase, so it is probable that the Mo underwent the same type of deformation as the Al did when forming hillocks. Since only a vacuum heat treatment was used, this result could be constrained, and Mo may have stability problems in an oxygen and nitrogen-containing atmosphere. Another weakness of the Mo is its low electrical conductivity in comparation with Al thin films.

IV. Conclusion

This paper characterizes the stability of the multilayer system Si substrate/AlN/Ti-Mo/$Al_{0.8}Sc_{0.2}N$/TE for different annealing temperature conditions. As a top metallization Al, AlSi, Mo/Al, and Mo were tested. Hillock formation is observed for all TE materials except Mo. The formation of voids is observed only in Al TE films. The maximum depth of the voids is 211 nm for the sample annealed at 450 °C for 30 min. Molybdenum is established as the most reliable metallization material for AlScN because it does not show any hillock or void formation in the annealing range of 100 °C to 450 °C. However, this finding may be limited because a vacuum heat treatment was used, and Mo might have stability issues in an atmosphere containing oxygen and nitrogen. Another disadvantage of Mo is its low electrical conductivity.

The system with Mo TE is stable up to 1000 °C for 100 h and does not reveal any new phase formation on the piezolayer interfaces or any interlayer diffusion. An assessment of the crystal quality of the AlScN films before and after annealing showed insignificant variation in the FWHM value for the ω-scan.

The piezoelectric response was determined using piezo-cantilevers made on the structures with Mo TE. Piezoelec-tric transverse coefficient $e_{31,f}$ value location-dependent of the piezo-cantilevers on the wafer was observed. The value is sensitive to not only the Sc concentration in the film but also AlScN grain tilt and local film stress. The films showed enhanced piezoresponce after annealing at 800 °C for 100–300 h. An increase in the absolute value of the

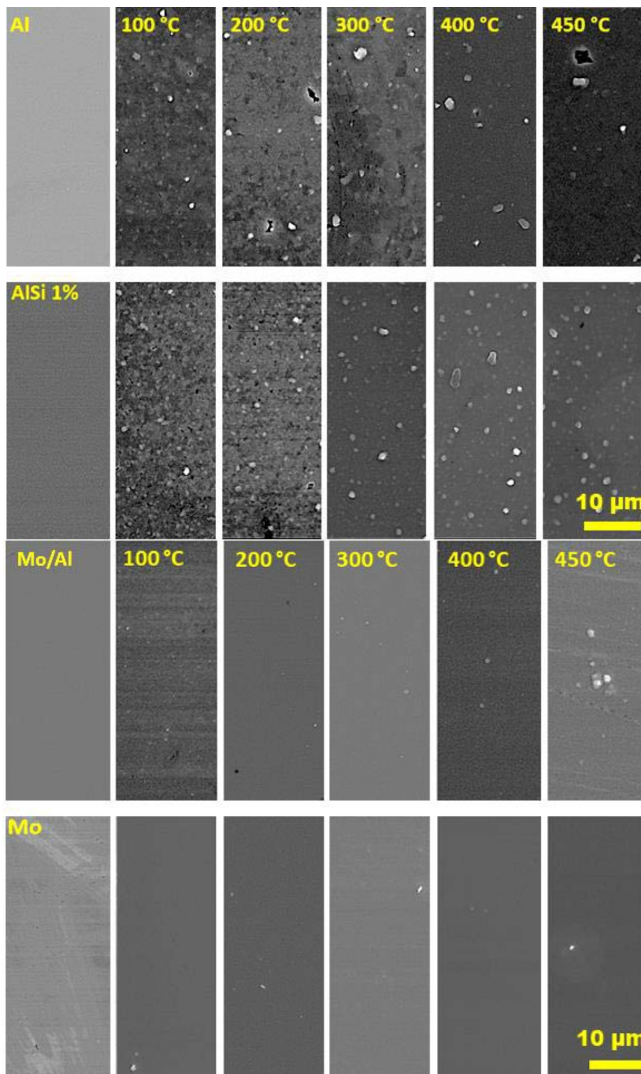

Fig. 10. SEM micrographs of the top metallization surfaces. Annealing time for all the samples is 30 min.

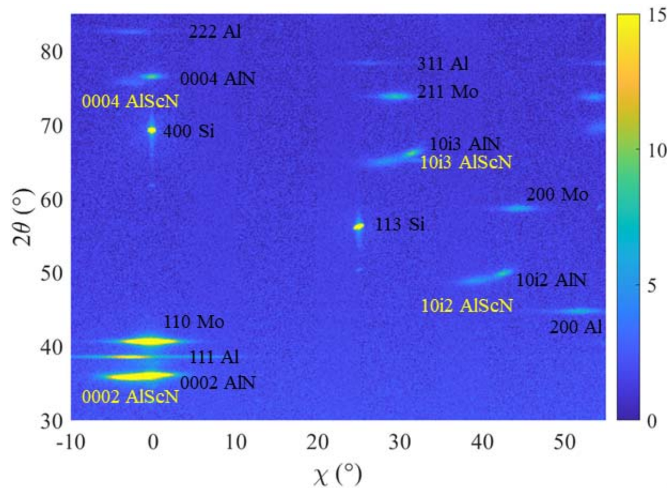

Fig. 11. Measured χ-2θ map of the as-deposited samples for the Si substrate/AlN/Ti-Mo/$Al_{0.8}Sc_{0.2}N$/Al structure.

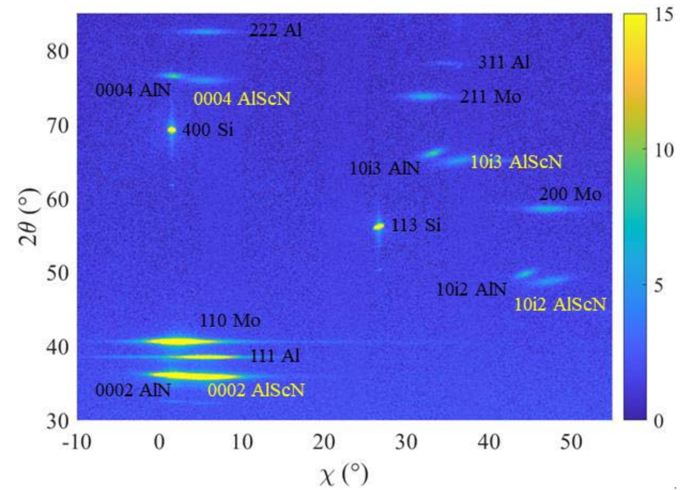

Fig. 12. Measured χ-2θ map for the structure Si substrate/AlN/Ti-Mo/$Al_{0.8}Sc_{0.2}N$/Al after annealing at 450 °C for 50 h.

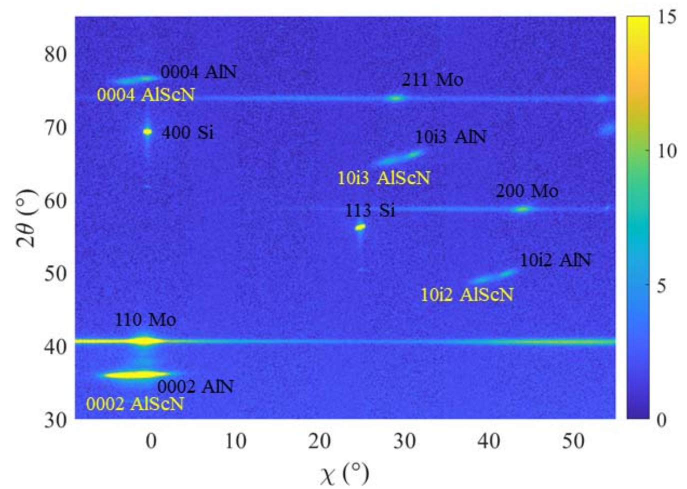

Fig. 13. Measured χ-2θ map of the as-deposited samples for the Si substrate/AlN/Ti-Mo/$Al_{0.8}Sc_{0.2}N$/Mo structure.

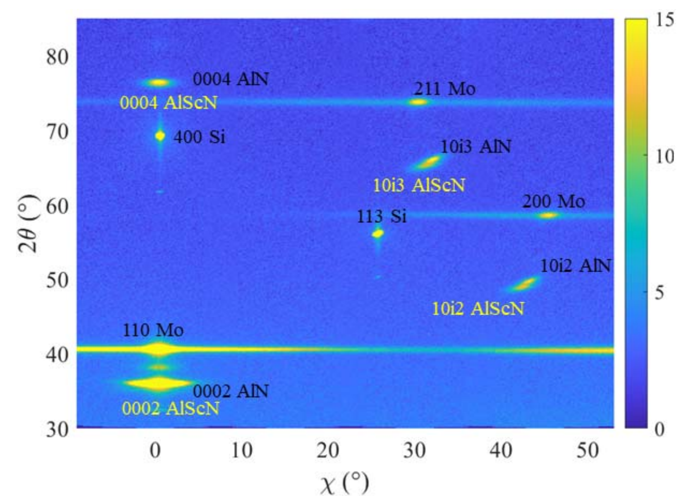

Fig. 14. Measured χ-2θ map for the structure Si substrate/AlN/Ti-Mo/$Al_{0.8}Sc_{0.2}N$/Mo after annealing at 450 °C for 50 h.

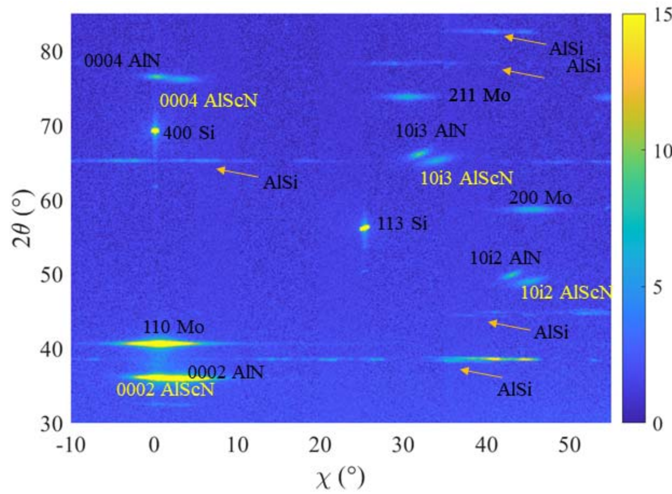

Fig. 15. Measured χ-2θ map of the as-deposited samples for the Si substrate/AlN/Ti-Mo/$Al_{0.8}Sc_{0.2}N$/AlSi structure.

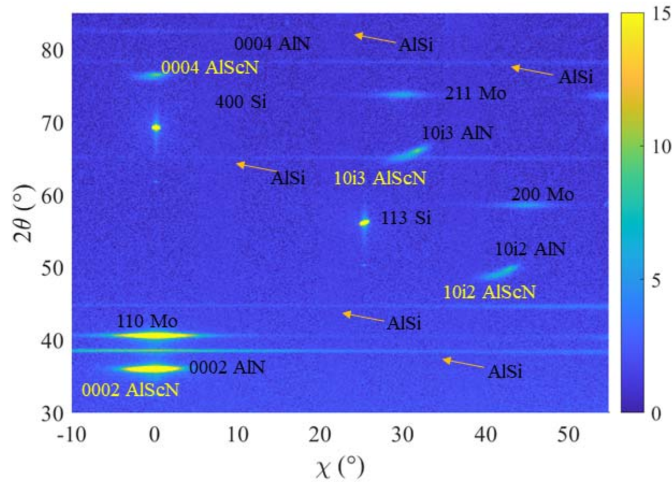

Fig. 16. Measured χ-2θ map for the structure Si substrate/AlN/Ti-Mo/$Al_{0.8}Sc_{0.2}N$/AlSi after annealing at 450 °C for 50 h.

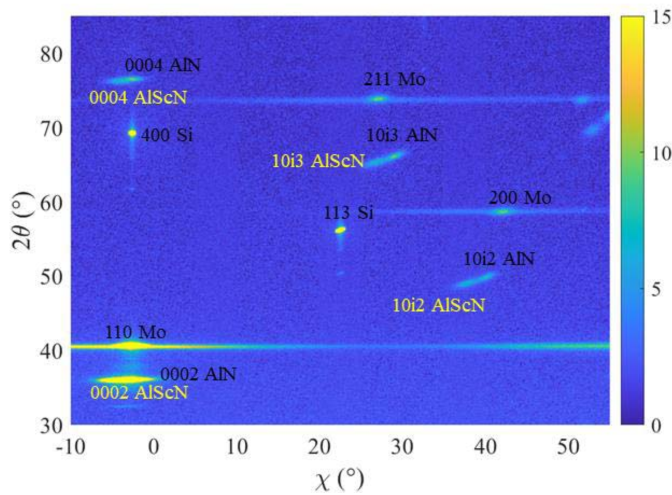

Fig. 17. Measured χ-2θ map of the as-deposited samples for the Si substrate/AlN/Ti-Mo/$Al_{0.8}Sc_{0.2}N$/Mo-Al structure.

piezoelectric transverse coefficient $e_{31,f}$ is not accompanied by any improvement in the crystalline structure, as evidenced by the FWHM values. Changes in the piezoelectric transverse coefficient after annealing were explained by changes in the configuration of the AlScN alloy.

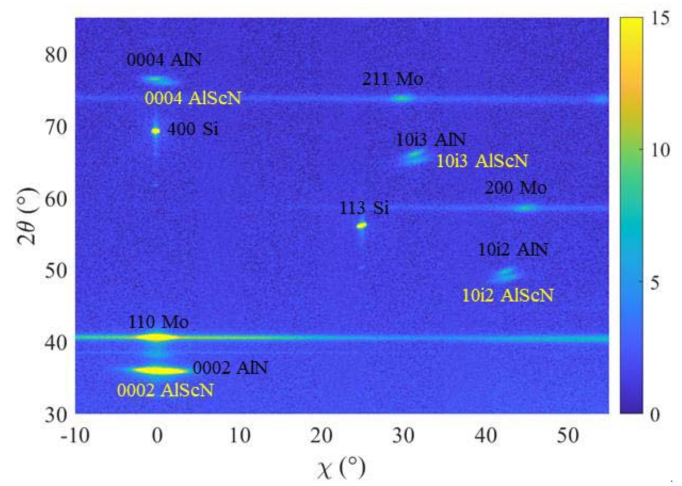

Fig. 18. Measured χ-2θ map for the structure Si substrate/AlN/Ti-Mo/$Al_{0.8}Sc_{0.2}N$/Mo-Al after annealing at 450 °C for 50 h.

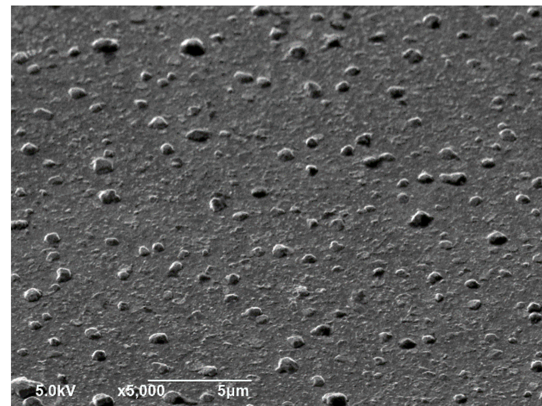

Fig. 19. Mo surface after annealing of the structure for 100 h at 1000 °C.

APPENDIX

Appendix A: Supplementary figures 10–19.

ACKNOWLEDGMENT

The authors acknowledge the provision of facilities and technical support by Aalto University OtaNano – Micronova Nanofabrication Centre, Nanomicroscopy Center, and VTT Technical Research Centre of Finland. The authors declare no conflict of interest.

REFERENCES

[1] C. Fei *et al.*, "AlN piezoelectric thin films for energy harvesting and acoustic devices," *Nano Energy*, vol. 51, pp. 146–161, Sep. 2018.

[2] S. Broeker, S. Fichtner, S. Bette, S. Tiedke, S. Tappertzhofen, and B. Wagner, "$Al_{1-X}Sc_XN$ thin films for pyroelectric IR detectors," in *Proc. MikroSystemTechnik Congr.*, Berlin, Germany, Oct. 2019, pp. 1–4.

[3] A. Ding *et al.*, "Investigation of temperature characteristics and substrate influence on AlScN-based SAW resonators," in *Proc. IEEE Int. Ultrason. Symp. (IUS)*, Kobe, Japan, Oct. 2018, pp. 1–9.

[4] M. Akiyama, T. Kamohara, K. Kano, A. Teshigahara, Y. Takeuchi, and N. Kawahara, "Enhancement of piezoelectric response in scandium aluminum nitride alloy thin films prepared by dual reactive cosputtering," *Adv. Mater.*, vol. 21, no. 5, pp. 593–596, Feb. 2009.

[5] M. Clement, V. F. J. Olivares, T. Mirea, J. Olivares, and E. Iborra, "Effects of post-deposition vacuum annealing on the piezoelectric properties of AlScN thin films sputtered on 200 mm production wafers," in *Proc. IEEE Int. Ultrason. Symp. (IUS)*, Kobe, Japan, Oct. 2018, pp. 1–4.

[6] S. Mertin *et al.*, "Enhanced piezoelectric properties of C-axis textured aluminium scandium nitride thin films with high scandium content: Influence of intrinsic stress and sputtering parameters," in *Proc. IEEE Int. Ultrason. Symp. (IUS)*, Washington, DC, USA, Sep. 2017, pp. 1–4.

[7] S. Fichtner *et al.*, "Identifying and overcoming the interface originating C-axis instability in highly Sc enhanced AlN for piezoelectric microelectromechanical systems," *J. Appl. Phys.*, vol. 122, no. 3, Jul. 2017, Art. no. 035301.

[8] P. M. Mayrhofer, P. Persson, A. Bittner, and U. Schmid, "Properties of $Sc_X Al_{1-X} N$ (X= 0.27) thin films on sapphire and silicon substrates upon high temperature loading," *Microsyst. Technol.*, vol. 22, no. 7, pp. 1679–1689, 2016.

[9] J.-C. Yang, X.-Q. Meng, C.-T. Yang, and W.-J. Fu, "Influence of N_2/Ar-flow ratio on crystal quality and electrical properties of ScAlN thin film prepared by DC reactive magnetron sputtering," *Appl. Surf. Sci.*, vol. 282, pp. 578–582, Oct. 2013.

[10] V. Felmetsger, M. Mikhov, M. Ramezani, and R. Tabrizian, "Sputter process optimization for $Al_{0.7}Sc_{0.3}N$ piezoelectric films," in *Proc. IEEE Int. Ultrason. Symp. (IUS)*, Glasgow, U.K., Oct. 2019, pp. 2600–2603.

[11] Q. Wang, Y. Lu, S. Mishin, Y. Oshmyansky, and D. A. Horsley, "Design, fabrication, and characterization of scandium aluminum nitride-based piezoelectric micromachined ultrasonic transducers," *J. Microelectromech. Syst.*, vol. 26, no. 5, pp. 1132–1139, Oct. 2017.

[12] M. Schneider, M. DeMiguel-Ramos, A. J. Flewitt, E. Iborra, and U. Schmid, "Scandium aluminium nitride-based film bulk acoustic resonators," *Multidisciplinary Digit. Publishing Inst. Proc.*, vol. 1, no. 4, p. 305, Aug. 2017.

[13] C. Höglund *et al.*, "Wurtzite structure $Sc_{1-X}Al_X N$ solid solution films grown by reactive magnetron sputter epitaxy: Structural characterization and first-principles calculations," *J. Appl. Phys.*, vol. 107, no. 12, Jun. 2010, Art. no. 123515.

[14] C. Höglund, J. Bareño, J. Birch, B. Alling, Z. Czigány, and L. Hultman, "Cubic $Sc_{1-X}Al_X N$ solid solution thin films deposited by reactive magnetron sputter epitaxy onto ScN(111)," *J. Appl. Phys.*, vol. 105, no. 11, Jun. 2009, Art. no. 113517.

[15] E. Österlund, "Deposition and characterization of aluminum nitride thin films for piezoelectric MEMS," Ph.D. dissertation, Aalto Univ., Espoo, Finland, 2020.

[16] E. Österlund *et al.*, "Stability and residual stresses of sputtered Wurtzite AlScN thin films," *J. Phys. Rev. Mater.*, Jan. 2020.

[17] T. Laurila, V. Vuorinen, M. Paulasto-Kröckel, M. Turunen, T. T. Mattila, and J. Kivilahti, *Interfacial Compatibility in Microelectronics: Moving Away From the Trial and Error Approach*. London, U.K.: Springer, 2012.

[18] J. L. Schroeder, B. Saha, M. Garbrecht, N. Schell, T. D. Sands, and J. Birch, "Thermal stability of epitaxial cubic-TiN/(Al, Sc) N metal/semiconductor superlattices," *J. Mater. Sci.*, vol. 50, no. 8, pp. 3200–3206, Apr. 2015.

[19] C. B. Karuthedath, A. T. Sebastian, J. Saarilahti, T. Sillanpaa, and T. Pensala, "Design and fabrication of aluminum nitride piezoelectric micromachined ultrasonic transducers for air flow measurements," in *Proc. IEEE Int. Ultrason. Symp. (IUS)*, Glasgow, U.K., Oct. 2019, pp. 2489–2492.

[20] S. Fichtner, N. Wolff, F. Lofink, L. Kienle, and B. Wagner, "AlScN: A III-V semiconductor based ferroelectric," *J. Appl. Phys.*, vol. 125, no. 11, Mar. 2019, Art. no. 114103.

[21] K. T. Raić, "An explanation of hillock growth in thin al films," *Surf. Eng.*, vol. 32, no. 11, pp. 823–828, Nov. 2016.

[22] N. Z. Liu and Y. Liu, "Suppressing hillock formation in Si-supported pure Al films," *Mater. Res. Exp.*, vol. 5, no. 4, Apr. 2018, Art. no. 046403.

[23] S.-J. Hwang, J.-H. Lee, C.-O. Jeong, and Y.-C. Joo, "Effect of film thickness and annealing temperature on hillock distributions in pure Al films," *Scripta Mater.*, vol. 56, no. 1, pp. 17–20, Jan. 2007.

[24] Y. Lu *et al.*, "Elastic modulus and coefficient of thermal expansion of piezoelectric $Al_{1-X}Sc_X N$ (up to X = 0.41) thin films," *APL Mater.*, vol. 6, no. 7, Jul. 2018, Art. no. 076105.

[25] W. Fang and C.-Y. Lo, "On the thermal expansion coefficients of thin films," *Sens. Actuators A, Phys.*, vol. 84, no. 3, pp. 310–314, Sep. 2000.

[26] K. Wang and R. R. Reeber, "The role of defects on thermophysical properties: Thermal expansion of V, Nb, Ta, Mo and W," *Mater. Sci. Eng., R, Rep.*, vol. 23, no. 3, pp. 101–137, Jul. 1998.

[27] I.-M. Park, S.-J. Hwang, J.-H. Lee, and Y.-C. Joo, "Effect of effective modulus on hillock formations in Al lines on glass," *Met. Mater. Int.*, vol. 15, no. 4, pp. 661–664, Aug. 2009.

[28] B. Bacconnier, G. Lormand, M. Papapietro, M. Achard, and A. M. Papon, "A study of heating rate and texture influences on annealing hillocks by a statistical characterization of Al thin-film topography," *J. Appl. Phys.*, vol. 64, no. 11, pp. 6483–6489, 1988.

[29] S. Franssila, *Introduction to Microfabrication*. Hoboken, NJ, USA: Wiley, 2010.

[30] A. Mazzalai, D. Balma, N. Chidambaram, L. Jin, and P. Muralt, "Simultaneous piezoelectric and ferroelectric characterization of thin films for MEMS actuators," in *Proc. Joint IEEE Int. Symp. Appl. Ferroelectr. Workshop Piezoresponse Force Microscale (ISAF/PFM)*, Prague, Czech Republic, Jul. 2013, pp. 363–366.

[31] D. Deniz, J. M. E. Harper, J. W. Hoehn, and F. Chen, "Tilted fiber texture in aluminum nitride thin films," *J. Vac. Sci. Technol. A, Vac., Surf., Films*, vol. 25, no. 4, pp. 1214–1218, 2007.

[32] S. Wu, M. Y. Wu, J.-L. Huang, and D.-F. Lii, "Characterization and piezoelectric properties of reactively sputtered (Sc, Al)N thin films on diamond structure," *Int. J. Appl. Ceram. Technol.*, vol. 11, no. 5, pp. 894–900, Sep. 2014.

[33] P. Daoust, P. Desjardins, R. A. Masut, V. Gosselin, and M. Côté, "*Ab initio* piezoelectric properties of $Al_{0.5}Sc_{0.5}N$: Impact of alloy configuration on the $d_{33,f}$ piezoelectric strain coefficient," *Phys. Rev. Mater.*, vol. 1, no. 5, Oct. 2017, Art. no. 055402.

[34] D. F. Urban, O. Ambacher, and C. Elsässer, "First-principles calculation of electroacoustic properties of wurtzite (Al, Sc) N," 2020, *arXiv:2002.08143*. [Online]. Available: http://arxiv.org/abs/2002.08143